An effective Q-compensation method for Fourier finite-difference wave-equation migration in tilted transversely isotropic media

Chen Tang, Jianming Sheng, Jian Mao, Yang He and Bin Wang, TGS Nopec Geophysical Company*

Summary

When a seismic wave propagates in the subsurface of the earth, its energy can be attenuated. This has a negative influence on both the amplitude and the phase of an image, especially when a geological body with large attenuation coefficients presents in the target survey area. Therefore, we need to compensate for the attenuation effect in wave propagation. The attenuation effect is generally frequency-dependent, so it is natural to incorporate the attenuation formula into the Fourier finite-difference wave-equation migration (FFD WEM) that also works in the frequency domain. The FFD WEM in tilted transversely isotropic (TTI) media involves three parts: a phase-shift, a thin-lens, and an FFD term. Compared to the traditional method that compensates the Q effect only in the thin-lens term, this paper involves two innovative parts: First, we incorporate a frequency-dependent velocity in all the three parts of the FFD WEM. As a result, the FFD coefficients are frequency-dependent and a complex-valued velocity is also included in the FFD term. Second, to obtain a stable Q-compensated wavefield, we design a filter in the frequency domain by comparing two propagating wavefields. The method aims at improving the Q-compensation accuracy for the FFD WEM in Q-TTI media, especially at relatively large propagation angles. Examples show that the proposed method can provide high-quality images for Q-TTI media.

Introduction

When a seismic wave propagates in the subsurface of the earth, its energy is gradually absorbed. This is caused by an intrinsic property of the medium that is known as seismic attenuation. It influences both the amplitude and the travel time of a propagating wave, which could further result in weak amplitudes and shifted phases in the image. When a geological structure with strong attenuation presents in the target survey area, the image's quality can be significantly reduced if the attenuation effect is not adequately compensated for. The strength of attenuation for a rock can be described by the seismic quality factor Q,

$$Q = 2\pi\left(\frac{E}{\delta E}\right), \tag{1}$$

where E is the energy of a seismic wave propagating in this rock and δE is the energy loss during one oscillation cycle of this wave. As shown in equation 1, a small Q value corresponds to a large attenuation effect. There are several ways to incorporate the attenuation effect into the wave equation. One of them is Futterman's (1962) formula that works in the frequency domain,

$$v_Q = v_{ref}\left[1 - \frac{1}{\pi Q}\ln\left(\frac{\omega}{\omega_{ref}}\right)\right]^{-1}\left(1 + \frac{i}{2Q}\right)^{-1}. \tag{2}$$

Here, v_Q and v_{ref} are the Q-dependent and reference velocities, respectively. ω and ω_{ref} are the frequency and reference frequency, respectively. In equation 2, the real part corresponds to the phase difference and the imaginary part corresponds to the amplitude difference. To compensate the attenuation, we need to keep the phase term to match the travel time and take a conjugate of the amplitude term to compensate the amplitude loss (e.g., Zhang et al., 2010). Equation 2 automatically separates the phase and amplitude terms, which facilitates constructing the Q-compensated formula,

$$v_{Q-inv} = v_{ref}\left[1 - \frac{1}{\pi Q}\ln\left(\frac{\omega}{\omega_{ref}}\right)\right]^{-1}\left(1 - \frac{i}{2Q}\right)^{-1}, \tag{3}$$

where v_{Q-inv} is the Q-compensated velocity. This is an important advantage of Futterman's formula over the generalized standard linear solid (GSLS) model (e.g., Carcione et al., 1988) that uses the strain and stress relaxation times to replace the parameter Q and does not separate the phase and amplitude effects.

Futterman's formula is in the frequency domain; therefore, it needs an extra effort to incorporate it with the time-domain reverse time migration, which could significantly increase the computational time (e.g., Zhang et al., 2010; Zhu et al., 2014), but it is well suited for the Fourier finite-difference (FFD) wave-equation migration (WEM) (Distow, 1994) that also works in the frequency domain. Some previous work about the FFD WEM in tilted transversely isotropic (TTI) media can be found in the work of Valenciano et al. (2009), Hua et al. (2010, 2013), and Tang et al. (2019). Shen et al. (2018) and Valenciano et al. (2011) also use Futterman's formula in their WEM approaches. The TTI FFD WEM involves three terms: phase-shift, thin-lens and FFD. We incorporate Futterman's formula into all three terms. Compared to the traditional method that involves the FFD in the second term only, this gives more accurate simulation of the attenuation at relatively large angles (e.g., above 45°). Because of involving v_{Q-inv} (in equation 3) in the Q-compensated wave equation with an increased dominant frequency and amplitudes, the implementation is not stable. To address this, we design a filter by comparing two propagating wavefields.

Theory

Defining the slowness vector as $\mathbf{s} = (S_x, S_y, S_z)$, the TTI FFD WEM formula can be written as (e.g., Hua et al., 2013)

$$\bar{S}_z = S_{z0} + \sqrt{\left(\frac{v_p}{v_{p0}}\right)^2 - \left(S_x^2 + S_y^2\right)} - \frac{v_p}{v_{p0}} - \sum_{n=x,y,m,p} \frac{c_n S_n + a_n S_n^2}{1 - b_n S_n^2 - d_n S_n}, \tag{4}$$

where $\bar{S}_z$ is an estimation of S_z. S_{z0} is the S_z in the normal direction and can be theoretically calculated. v_p is the velocity and v_{p0} is the reference velocity. (a, b, c, d) are the coefficients in the *x*-, *y*-, *m*- and *p*-directions that correspond to 0°, 45°, 90° and -45°, respectively. Equation 4 can be rewritten as (Tang et al. 2019)

$$\frac{\partial}{\partial z} = -i\sqrt{\left(\frac{\omega}{v_{p0}}\right)^2 - \left(k_x^2 + k_y^2\right)} - i\omega\left(\frac{S_{z0}}{v_p} - \frac{1}{v_{p0}}\right) - \sum_{n=x,y,m,p} \frac{c_n \frac{\partial}{\partial n} + a_n \frac{v_p}{-i\omega}\frac{\partial^2}{\partial n^2}}{1 - b_n\left(\frac{v_p}{-i\omega}\right)^2 \frac{\partial^2}{\partial n^2} - d_n \frac{v_p}{-i\omega}\frac{\partial}{\partial n}}, \tag{5}$$

where $\mathbf{k} = (k_x, k_y, k_z)$ is the wavenumber. The right side of equation 5 involves three components: phase-shift, thin lens and FFD. Incorporating equation 2 into equation 5 gives

$$\frac{\partial}{\partial z} = -i\sqrt{\left[\frac{\omega}{v_{Q0}(\omega)}\right]^2 - \left(k_x^2 + k_y^2\right)} - i\omega\left[\frac{S_{z0}}{v_Q(\omega)} - \frac{1}{v_{Q0}(\omega)}\right] - \sum_{n=x,y,m,p} \frac{c_n(\omega)\frac{\partial}{\partial n} + a_n(\omega)\frac{v_Q(\omega)}{-i\omega}\frac{\partial^2}{\partial n^2}}{1 - b_n(\omega)\left[\frac{v_Q(\omega)}{-i\omega}\right]^2 \frac{\partial^2}{\partial n^2} - d_n(\omega)\frac{v_Q(\omega)}{-i\omega}\frac{\partial}{\partial n}}. \tag{6}$$

Equation 6 shows that the coefficients in the FFD term are frequency-dependent; they are obtained at each frequency from a pre-calculated coefficient table that is calculated from the method proposed by Tang et al. (2019), which combines linear and nonlinear inversions to improve the accuracy of the coefficient estimation. The velocity in the FFD term is also complex-valued; if we approximate it as its modulus, equation 6 is simplified to the corresponding formula of Tang et al. (2020).

Figure 1 shows a comparison between three wavefield snapshots that are obtained from modeling without attenuation in (a), with partial attenuation in (b), and with equation 6 in (c), respectively. The partial attenuation in Figure 1b denotes a traditional method that includes v_Q (calculated from equation 2) only in the thin-lens term of the FFD WEM propagator, which is simple and also less expensive than the proposed method in equation 6. The example uses a constant 2D Q-TTI model. The P-velocity is 2000 m/s and Q is 20. The anisotropic parameters epsilon and delta are 0.25 and 0.15, respectively, and the polar angle theta is 30°. Because of incorporating attenuation in the propagator, both Figures 1b and 1c show an amplitude decay and phase shifts when compared to Figure 1a. Comparing Figures 1b and 1c, we can observe both amplitude and phase differences, especially in the areas highlighted by green ovals. As is shown in Figure 1c, the proposed method gives a more reasonable result because of the two phenomena: 1) Compared to Figure 1c, the amplitude in Figure 1b (with partial attenuation) is not well attenuated at relatively large dip angles (see the area highlighted by the green oval). 2) With an increased dip angle, the phase in Figure 1b generally becomes more similar to that in Figure 1a (without attenuation). This is because the modeling accuracy with only partial attenuation generally decreases with an increased dip angle.

Matching filter

A combination of equations 2 and 6 gives a simulation of the attenuation effect. To compensate this effect, we need to use v_{Q-inv} calculated by equation 3 to replace v_Q in equation 6,

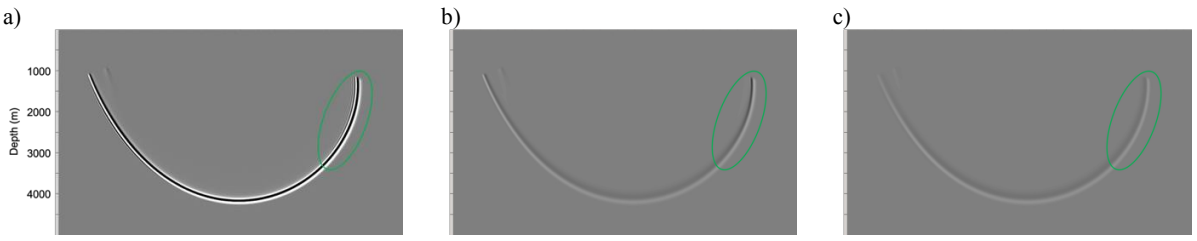

Figure 1: Comparison of wavefield snapshots without attenuation in (a), with attenuation only in the thin-lens term in (b), and with the proposed method in equation 6 in (c). An angle mute at 75° has been applied to all these snapshots. Here, the angle is measured from the line between the source and the point.

$$\frac{\partial}{\partial z} = L_1\left(v_{Q-inv}\right) + L_2\left(v_{Q-inv}\right) + L_3\left(v_{Q-inv}\right), \quad (7)$$

where L_1, L_2 and L_3 represent the phase-shift, thin-lens and FFD terms, respectively. However, because equation 3 describes compensation of the Q effect including boosting the amplitude, involving $v_{Q\text{-}inv}$ in the FFD (L_3) term causes instability in the implementation of equation 7. To obtain a stable Q-compensated wavefield, we refer to the work of Xie et al. (2015) and design a matching filter

$$F^2(\omega, \mathbf{x}) = \left| \frac{u_{inv-2}(\omega, \mathbf{x})}{u_{inv-1}(\omega, \mathbf{x})} \right|^2, \quad (8)$$

where **x** is the location, u_{inv-1} is obtained from

$$\frac{\partial}{\partial z} = L_1\left(v_{Q-inv}\right) + L_2\left(v_{Q-inv}\right) + L_3\left(v_{Q}\right), \quad (9)$$

and u_{inv-2} is obtained from

$$\frac{\partial}{\partial z} = L_1\left(v_{Q-inv}\right) + L_2\left(v_{Q-inv}\right) + L_3\left(\left|v_{Q-inv}\right|\right). \quad (10)$$

Neither equation 9 nor 10 uses v_{Q-inv} as the velocity in the FFD (L_3) term; therefore, they are stable. Because v_Q and v_{Q-inv} are conjugate, instead of using equation 7 to calculate u_{inv}, we can approximate u_{inv} as

$$u_{inv} = F^2(\omega, \mathbf{x})\, u_{inv-1}. \quad (11)$$

A threshold λ^2 needs be applied to $F^2(\omega, \mathbf{x})$ in order to maintain the stability, and then equation 11 becomes

$$u_{inv} = \min\left[\lambda^2, F^2(\omega, \mathbf{x})\right] u_{inv-1}. \quad (12)$$

Equation 12 can also be approximated to

$$u_{inv} = \min\left[\lambda, \left|F(\omega, \mathbf{x})\right|\right] u_{inv-2}, \quad (13)$$

where λ is a real number. Note that, the approach of Xie et al. (2015) is designed for the Q-compensated RTM and the filter in their paper is calculated by comparing propagating wavefields with and without Q in the frequency domain. Therefore, applying this method to the time-domain RTM requires extra computational time to transform the wavefields between the time and frequency domains. This issue is easily avoided as the FFD WEM works in the frequency domain.

Examples

We show image comparisons for 2D synthetic (Figure 2) and 3D real data (Figure 3) examples below. The synthetic data used to produce Figure 2 is generated from a Q-TTI model in which the TTI part is modified from the BPTTI model. The main modification adds a scaled image to the velocity model, as we do not use a density model for generation of the synthetic data. The background Q model is embedded with a strong attenuation body with a Q value of 20 (Figure 2a). Figure 2b shows the image without Q compensation. We observe the weak amplitudes in the middle part (highlighted by the blue box) which approximately corresponds to the area in and under the Q body in Figure 2a. The attenuation has been adequately compensated for after using the proposed method, which is shown in Figure 2c. If we put the two images at the same location and shift them back and forth, phase shifts can also be observed. A comparison of vertical-wavenumber spectra is presented in Figure 2d, which shows that after Q compensation, the dominant frequency moves to a higher one.

We then apply 3D Q-TTI FFD WEM to a field dataset from narrow-azimuth acquisition in the Porcupine Basin (Crean Survey). Besides the strongly attenuative structure, the value of which is estimated from comparing spectra at the surface, we also add background Q values to the model. Figure 3b (with the proposed Q-compensation method) presents a better image than Figure 3a (without Q compensation). For example, we can observe that the weak amplitudes in the area highlighted by the green box in Figure 3a; the Q effect is compensated for by using the proposed method; see the area highlighted by the red box in Figure 3b. Comparison of vertical-wavenumber spectra is shown in Figure 3c, which presents that the image with the proposed Q-compensation method contains a larger weight of high-frequency components than the one without Q compensation.

Conclusions

We develop an improved method for the FFD WEM in Q-TTI media by incorporating the frequency-dependent, complex-valued velocity calculated by Futterman's formula into all the three terms (phase-shift, thin-lens and FFD) of its propagator. In this method, the propagator has a unique group of coefficients at each frequency and the FFD term also involves a complex-valued velocity. Compared to the traditional method that involves Q compensation only in the thin-lens term, the proposed method improves the simulation accuracy at relatively large propagation angles. To solve the instability issue in the Q-compensated propagator, which is introduced by including the complex-valued velocity in the FFD term, a matching filter is calculated by comparing two propagation wavefields in the frequency domain. Examples show that the proposed method adequately compensates for the attenuation and provides high-quality images for 2D synthetic and 3D real datasets.

Acknowledgments

The authors thank TGS Nopec Geophysical Company for the permission to publish this work. We are also grateful to S. Spoors, C. J. VanSchuyver and A. C. Ramirez for reviewing this paper.

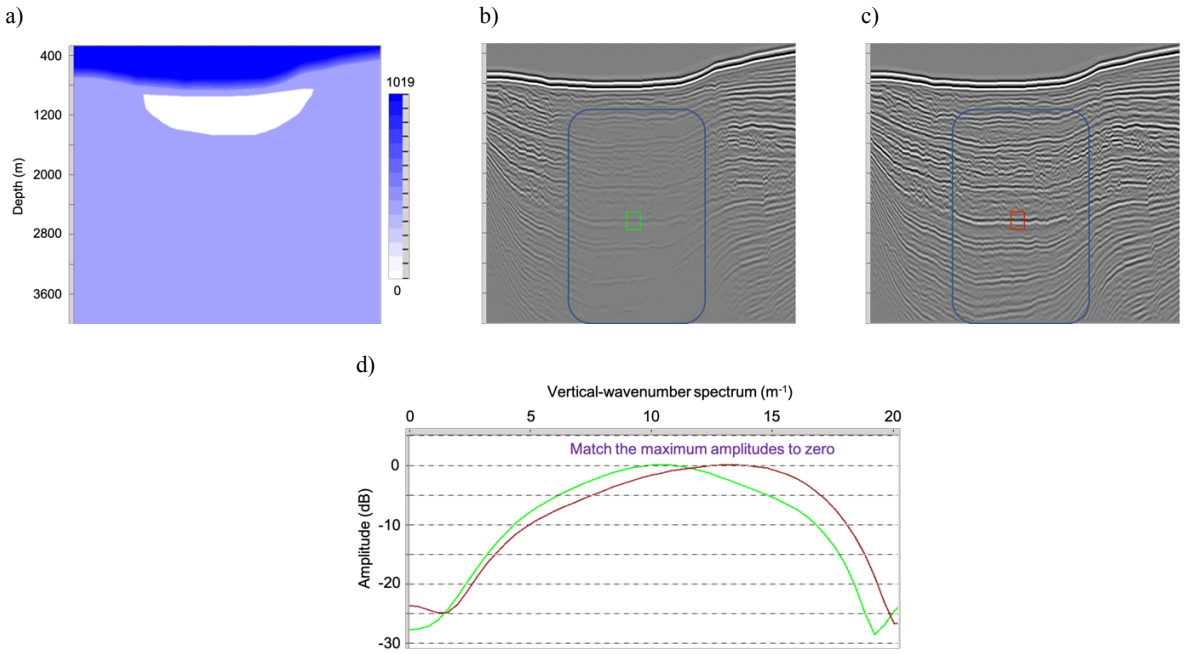

Figure 2: Comparison of FFD WEM images using the synthetic data from a 2D Q-TTI model. The TTI part is modified from the BP TTI model, and the Q model is presented in (a) where the Q value of the target attenuation body (in white color) is 20. (b) shows the image without Q compensation. (c) shows the image with the proposed Q-compensation method. (d) shows comparison of the vertical-wavenumber spectra. The green and red spectra correspond to the areas highlighted by the green and red boxes in (b) and (c), respectively. Here, we match the maximum values of the two spectra to zero, so the amplitude numbers are not the absolute values. If we use the absolute values, the green spectrum would generally be lower than the red spectrum in the presented range.

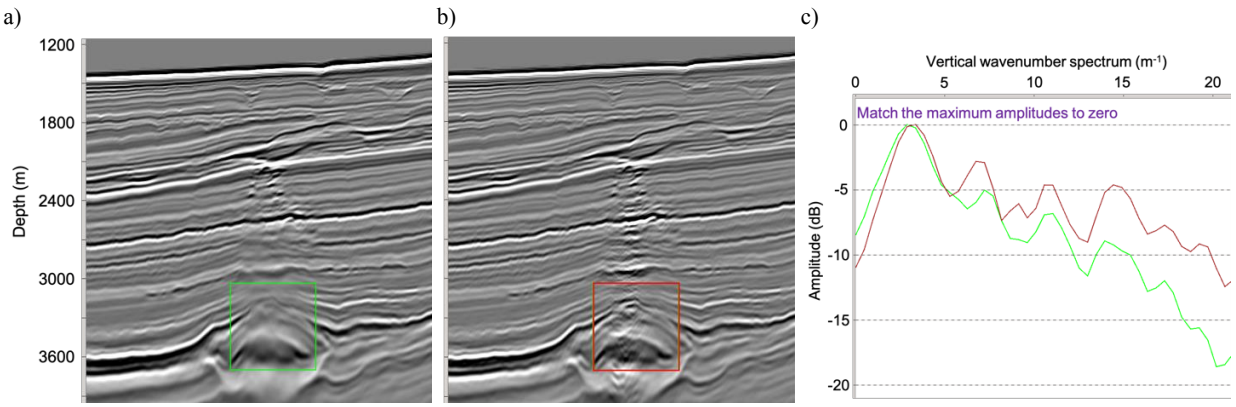

Figure 3: Comparison of FFD WEM images using a 3D field dataset from Crean Survey. (a) presents the image without Q compensation. (b) presents the image with the proposed Q-compensation method. (c) presents a comparison of the vertical-wavenumber spectra. The green and red curves in (c) correspond to the areas highlighted by the green and red boxes in (a) and (b), respectively. Note that, the amptliude numbers are not the absolute values and please refer to the caption for Figure 2d.

REFERENCES

Carcione, J. M., D. Kosloff, and R. Kosloff, 1988, Wave propagation simulation in a linear viscoacoustic medium: Geophysical Journal International, **93**, 393–401, doi: https://doi.org/10.1111/j.1365-246X.1988.tb02010.x.

Distow, D., 1994, Fourier finite-difference migration: Geophysics, **59**, 623–631.

Futterman, W. I., 1962, Dispersive body waves: Journal of Geophysical Research, **67**, 5279–5291, doi: https://doi.org/10.1029/JZ067i013p05279.

Hua, B., P. Williamson, B. Duquet, and J. Benamou, 2010, 3D TTI implicit finite difference migration with nonlinear optimized four-direction splitting expansion: 80th Annual International Meeting, SEG, Expanded Abstracts, 2082–2085.

Hua, B., P. Williamson, B. Duquet, and H. Houllevigue, 2013, High-order and high-accuracy 3D Fourier finite difference depth migration with an optimally reduced coefficient table for tilted transversely isotropic media: 83rd Annual International Meeting, SEG, Expanded Abstracts, 3794–3798, doi: https://doi.org/10.1190/segam2013-1052.1.

Shen, Y., B. Biondi, and R. Clapp, 2018, Q-model building using one-way wave-equation migration Q analysis — Part 1: Theory and synthetic test: Geophysics, **83**, no. 2, S93–S109, doi: https://doi.org/10.1190/geo2016-0658.1.

Tang, C., Y. He, J. Mao, and J. Sheng, 2019, Fourier finite-difference wave-equation migration in tilted transversely isotropic media with an improved solution for coefficient estimation: 89th Annual International Meeting, SEG, Expanded Abstracts, 4292–4296, doi: https://doi.org/10.1190/segam2019-3214439.1.

Tang, C., Y. He, J. Sheng, and B. Wang, 2020, Q-compensated Fourier finite-difference wave equation migration in tilted transversely isotropic media: Presented at 82nd EAGE Conference and Exhibition.

Xie, Y., J. Sun, Y. Zhang, and J. Zhou, 2015, Compensating for visco-acoustic effects in TTI reverse time migration: 85th Annual International Meeting, SEG, Expanded Abstracts, 3996–4001, doi: https://doi.org/10.1190/segam2015-5855445.1.

Valenciano, A. A., C. C. Cheng, N. Chemingui and S. Brandsberg-Dahl, 2009, Fourier finite-difference migration for 3D TTI media: 71st Conference and Exhibition, EAGE, Extended Abstracts, P065.

Valenciano, A. A., N. Chemingui, D. Whitmore, and S. Brandsberg-Dahl, 2011, Wave equation migration with attenuation and anisotropy compensation: 81st Annual International Meeting, SEG, Expanded Abstracts, 232–236, doi: https://doi.org/10.1190/1.3627674.

Zhang, Y., P. Zhang, and H. Zhang, 2010, Compensating for visco-acoustic effects in reverse-time migration: 80th Annual International Meeting, SEG, Expanded Abstracts, 3160–3164, doi: https://doi.org/10.1190/1.3513503.

Zhu, T., J. M. Harris, and B. Bion, 2014, Q-compensated reverse-time migration: Geophysics, **79**, no. 3, S77–S87, doi: https://doi.org/10.1190/geo2013-0344.1.